Boosting Photocatalytic Efficiency of MoS2/CdS By Modulating Morphology

Yubing Sun (sunyb@ipp.ac.cn)
North China Electric Power University https://orcid.org/0000-0003-4931-8039
Jingting Xiao
North China Electric Power University
Xinshui Huang
North China Electric Power University
Peng Mei
North China Electric Power University
Huihui Wang
North China Electric Power University
Yubing Sun
North China Electric Power University

Research Article

Keywords: MoS2, CdS, photocatalytic reduction, U(VI)

Posted Date: December 15th, 2021

DOI: https://doi.org/10.21203/rs.3.rs-1041316/v1

Abstract

With the rapid development of nuclear-related industries in the world, the consequent environmental pollution of radionuclides has become an increasingly serious problem due to the great harm to environmental diversity and human health. The photocatalytic removal of radionuclide on CdS-based photocatalysts has been attracted widely attentions due to the suitable band gap and high photocatalytic efficiency. In this study, approximately 97.5% of U(VI) was photo-catalytically reduced into U(IV) by 2.5 wt% MoS_2/CdS composite within 15 min. After 5 cycles, 2.5 wt% MoS_2/CdS composite still exhibited the high removal efficiency of U(VI) under 50 min irradiation, indicating the good stability. The findings indicated that CdS-based catalyst has a great potential for the photocatalytic reduction of uranyl in actual environmental remediation.

1. Introduction

With the development of economy and society, mankind's demand for energy is seriously increasing year by year(Arunachalam &Fleischer 2008, Chu &Majumdar 2012, Jacobson 2009, Jacobson &Delucchi 2011). Nuclear energy as one of the most promising energy source has been widely used in countries of the world due to high energy density and clean energy(Graves et al. 2011, Jiang et al. 2018, Zhang et al. 2019). Uranium has extensively used in nuclear-related industries, which exhibits a great threat to the environmental diversity and human health(Andrews &Cahill 2013, Jiang et al. 2018, Zhang et al. 2019). Therefore, it is very important to remove these pollutants before releasing the environment. Various methods, including chemical precipitation(B. et al. 1998), ultrafiltration(Misra et al. 2009), photocatalysis(Chang et al. 2015, He et al. 2016) and adsorption(Dolatyari et al. 2016, Li et al. 2016), have been widely used to remove uranium from aqueous solutions(Xie et al. 2013b). The photocatalytic reduction of U(VI) into U(IV) by various photocatalyst is regarded as the promising method due to environmental friendly, low cost and high removal efficiency(Chang et al. 2015, Jiang et al. 2018, Qin et al. 2017, Wu et al. 2017).

CdS as a common photocatalyst has been widely investigated to photocatalytic removal of various environmental pollutants due to the feasible band gap (~2.4 eV) and high photocatalytic activity(He et al. 2016, Liu et al. 2013, Zong et al. 2010). CdS exhibits the different energy band structures due to the different crystal phases such as hexagonal and cubic structures, which determines the light absorption and redox ability of photogenerated charge carriers(Yin et al. 2016b, Zhang et al. 2014). However, the poor stability of CdS extends the light time prone to corrosion, which limits the actual environmental application(Chen et al. 2015, Li et al. 2019b, Wu et al. 2017). Various metal disulfides (e.g., MoS_2) have been extensively employed to increase electron transport, which are conducive to effectively separate electron-hole pairs and decrease band gaps(Xie et al. 2013a, Yin et al. 2016b). For instance, MoS_2/CdS composites have been widely used in energy storage (e.g., hydrogen/oxygen evolution reaction) and environmental cleanup (e.g., degradation of organics and photocatalytic removal of heavy metals and radionuclides)(Chen et al. 2015, Jiang et al. 2015, Jiang et al. 2018, Yin et al. 2016a, Zong et al. 2008).

However, few investigations concerning the photocatalytic reduction of U(VI) on MoS_2/CdS composites are available.

The objectives of this study are (1) to synthesize MoS_2/CdS composites and characterize them using TEM, XRD, FTIR, UV-vis UV-visible diffuse reflectance spectroscopy (DRS), photoluminescence (PL) spectra and Electrochemical impedance spectroscopy (EIS) techniques; (2) to investigate the photocatalytic reduction of U(VI) by MoS_2/CdS under different environmental conditions; (3) to demonstrate the interaction mechanism of U(VI) on MoS_2/CdS using quenching experiments, EPR and XPS techniques. These findings are very important for environmental scientists and material engineers to design metal sulfide-containing materials with high chemical stability and excellent removal performance towards various pollutants in actual environmental remediation.

2. Experimental

2.1 Materials

Cadmium acetate ($Cd(CH_3COOH)_2{\cdot}2H_2O$, Aladdin, 99.99% purity), ammonium molybdate ($(NH_4)_6Mo_7O_{24}{\cdot}4H_2O$, Aladdin, 99.99%), thiourea ($(NH_2)_2CS$, Aladdin, 99% purity), *N*-*N*-dimethylformamide (DMF) and ethanol were purchased from Tianjin Damao Chemical reagent Co., Ltd. Methanol (Me), tert-butanol (TBA), p-Benzoquinone (p-BQ) were obtained from Aladdin. All the reagents used were of analytical grade and used without further purification.

2.2 Synthesis of MoS_2/CdS nanoparticles

MoS_2/CdS composites were prepared by solvothermal method(Li et al. 2019b, Wu et al. 2017, Yin et al. 2016b). CdS nanospheres were firstly prepared by hydrothermal method(Chen et al. 2015). Briefly, 0.8529 g $(CH_3COO)_2H_2O$ and 1.2179 g $(NH_2)_2CS$ were dissolved in 40 mL deionized water under vigorous stirring and room temperature for 30 min. The mixture was added into 50 mL Teflon-lined stainless steel autoclave and heated at 140°C for 24 h and then cooled to room temperature. The orange CdS (inset in Figure 1a) was obtained by drying it at 80 ℃ for 12 h after washing with deionized water and ethanol three times and centrifuging it at 3000 rpm for 10 min. The synthesis process of MoS_2/CdS was as follows: Typically, 0.5 g of as-prepared CdS was dispersed in the mixed solvent (16.67 mL DMF and 8.33 mL H_2O) under ultrasound treatment for 30 min, then 0.0145 g $(NH_4)_6Mo_7O_{24}{\cdot}4H_2O$ and 0.0268 g of $(NH_2)_2CS$ were added simultaneously for 60 min. The suspension was heated at 200°C for 24 h and then cooling to room temperature under 100 mL Teflon-lined stainless steel autoclave. The MoS_2/CdS (~2.5 wt% MoS_2) composites were obtained by drying them at 60 ℃ for 12 h after washing with ethanol and deionized water several times. Additionally, 5 wt% MoS_2/CdS (Figure S1b) and 10 wt % MoS_2/CdS (Figure S1c) composites were also fabricated by adding two and four-fold amounts, respectively, of $(NH_4)_6Mo_7O_{24}{\cdot}4H_2O$ and $(NH_2)_2CS$.

2.3 Characterization

Transmission electron microscope (JEOL, JEM-2100F, Japan) and scanning electron microscope (Hitachi, s4800) was employed to determine morphological features. Fourier transferred infrared spectrometer (IRTracer-100 Shimadzu Corporation) were conducted using KBr disc method. Brewer-Emmett-Taylor (BET) surface area of samples was determined by TriStar II. XPS spectra were taken on an X-ray photoelectron spectroscope (Escalab 250xi instrument, Thermo ESCALAB) using monochromatic Al Kα radiation (225 W, 15 mA, 15 kV) and low-energy electron flooding for charge compensation. The crystallinity of as-prepared MoS_2/CdS was characterized using X-ray diffractometer (Rigaku Giegerflex D/Max B diffractometer with Cu-Kα radiation). EIS measurement was carried out on the CHI-660D electrochemical workstation. In the three-electrode system, Pt counter electrode in saturated Na_2SO_4 and a standard calomel reference electrode are used. PL spectra were conducted using RF-6000 photoluminescence emission spectrometer at 380 nm. The optical properties were measured by Shimadzu Corporation UV-2700 UV-Visible Light Photometer and UV-visible diffuse reflectance spectroscope (DRS, barium sulfate as the reflection standard).

2.4 Photoreduction of U(VI)

The photoreduction experiments were conducted in a photocatalytic reaction box (CEL-HXF 300, China Education Au-Light) and a Xenon lamp (150 W, as the light source) with a double-walled beaker with circulated water to keep the constant temperature. Briefly, 0.05 g of MoS_2/CdS was added 50 mL 20 mg/L UO_2^{2+} solution with a small amount of methanol. pH of the mixture was adjusted by adding small volumes of NaOH and HNO_3 solutions. The suspension was pre-introduced firstly N_2 2h and then reacted in the dark for 30 min remove dissolved oxygen from water and to achieve the adsorption equilibrium, respectively. After adsorption equilibrium, the mixtures were exposed in a photocatalytic reaction box under different time intervals (15, 30, 60, 90 and 120 min).

In the recycle experiment, the samples after photocatalytic reaction for 60 min were washed several times with deionized water, and dried it in vacuum at 60 ºC for 12 h, and then the dried powder was collected to conduct the photocatalytic experiment again and repeated five times.

In the quenching experiment, photoreduction experiments were conducted by separately adding methanol, TBA and p-BQ solution, which were used as radical scavengers for holes, ·OH and $\cdot O_2^-$ radical, respectively. After reaction, the suspension was centrifuged at 4000 r/min for 10 min, the concentration of uranium in supernatant was measured by UV-vis spectrophotometer at 650 nm.

3. Results And Discussion

3.1 Characterization

The morphology of as-prepared MoS_2/CdS was characterized by SEM and TEM images. Fig. 1a and 1b show SEM image of CdS and TEM image of 2.5 wt % MoS_2/CdS, respectively. The olive-like CdS had an irregular block-shape, rough surface and obvious aggregation(Chai et al. 2018, Chen et al. 2012). For 2.5 wt% MoS_2/CdS composite, the irregular flaky MoS_2 was anchored at the edge of CdS(Xu &Cao 2015, Zhang et al. 2018, Zong et al. 2010), As inset in Fig. 1a and 1b, the color of bright orange CdS was transformed into deep orange after adding MoS_2.

XRD analysis was used to characterize crystal structure of MoS_2/CdS (Fig. 1c). The diffraction peaks at 2θ = 24.9, 26.5, 28.3, 43.8, 48 and 52º corresponded to the (100), (002), (101), (110), (103) and (112) planes of cubic CdS, respectively(Alomar et al. 2019, Jin &Li 2020). The high diffraction peak intensity of (101) plane indicated the growth of CdS along (101) crystal plane(Wu et al. 2017). The large and sharp diffraction peak intensity of 2.5 wt% MoS_2/CdS showed the good crystallization. Compared to CdS, no obvious shift in the diffraction peak of MoS_2/CdS composites indicated the loading of MoS_2 rather than doping(He et al. 2016). However, no diffraction peak of MoS_2 may be due to the small content(Li et al. 2019b). No significant change in diffraction peaks after photocatalytic reaction indicated 2.5 wt% MoS_2/CdS composite with strong stability.

Figure 1d shows the FT-IR spectra of 2.5 wt% MoS_2/CdS nanocomposites before and after the reaction in the frequency range of 400 ~ 4000 cm^{-1}. The IR bands at 428 and 508 cm^{-1} corresponded to the stretching vibration of Mo-S and $(S\text{-}S)^{2-}$ bond, respectively(Habibi &Rahmati 2014). The stretching vibration of Cd-S bond and the bending vibration of H_2O were observed at 630 and 1572 cm^{-1}, respectively. The broad peak in the range of 3200 ~ 3500 cm^{-1} was related to the vibration of O-H bond(Khawula et al. 2016). After the reaction, no new bands and little shift indicated that main interaction mechanism of U(VI) on MoS_2/CdS composite was photoreduction rather than adsorption(Yan et al. 2009, Yuan et al. 2018).

Figure S2 shows nitrogen adsorption-desorption isotherms and corresponding pore size distribution curves of CdS and 2.5 wt% MoS_2/CdS composite. The IV-type adsorption isotherms showed H_3 hysteresis loop, indicating the aggregation of plate-like particles on slit-like pores(Misra et al. 2009, Sing et al. 1985). The main size distribution (~ 2 and 85 nm) suggested the formation of mesoporous and microporous 2.5 wt% MoS_2/CdS composite. From table S1, BET specific surface area of MoS_2/CdS composite (~8.8 m^2/g) was slightly higher than CdS (3.8 m^2/g) due to the increase of mesopore by adding MoS_2(Yu et al. 2014), which is beneficial to improve the catalytic performance due to accommodation of more surface active sites and promotion of the transport of charge carriers (Alomar et al. 2019, Di et al. 2016).

To study the light absorption characteristics, UV-vis DRS and PL spectra (at 500-700 nm) of 2.5 wt% MoS_2/CdS composite were showed in Fig. 2a and 2b, respectively. For CdS, a strong absorption band edge at ~ 530 nm corresponded to the inherent band gap absorption of hexagonal CdS(Li et al. 2019b,

Yin et al. 2016b). It is worth noting that the gradual increase of light absorption intensities in 580-800 nm with the increase of MoS_2 may be due to the color shift from bright orange into dark orange MoS_2/CdS composite(Zhang et al. 2014). According to the calculation of Tauc plots (Supporting information), the band gap of 2.5 wt% MoS_2/CdS composite (2.31 eV) was significantly lower than CdS (2.43 eV, inset of Fig. 2a) owing to charge transfer from CV of MoS_2 to CdS(Zong et al. 2010).

PL spectrum as an important tools provides important information of photo-generated electron-hole separation efficiency(Lin et al. 2017). The high PL intensity of CdS (Fig. 2b) indicated the high recombination centers due to trap-related states(Wu et al. 2017). The low PL intensity of 2.5 wt% MoS_2/CdS composite indicated low recombination of photogenerated electrons and holes(Yuan et al. 2018), which also reduce the photo-corrosion of CdS(Zong et al. 2008). The effective transfer of photogenerated electrons from CB of CdS into CB of MoS_2 indicated that the introduction of MoS_2 inhibited recombination of photogenerated electrons and holes, which significantly improved the photocatalytic activity(Yin et al. 2016a, Zhang et al. 2014).

To further understand the charge separation, the photocurrent responses of CdS and 2.5 wt% MoS_2/CdS under several intermittent full-light irradiation was showed in Figure 2c. The transient photocurrent of all samples quickly reached a constant value under continuous illumination(Jiang et al. 2015), whereas the photocurrent reached to 0 after close of irradiation. Compared to CdS (4.76 μA/cm^2), the high photocurrent density of 2.5 wt% MoS_2/CdS composite (31.13 μA/cm^2) indicated the effective inhibit recombination of photogenerated electrons and holes due to the formation of heterostructure(Chen et al. 2015, He et al. 2016).

As shown by Nyquist diagram of EIS spectrum in Fig. 2d, the semicircle related to charge transfer resistance (R_{ct}) is connected in parallel with a sub-layer capacitor (CPE)(Li et al. 2019a, Yu et al. 2014). Compared to CdS, the small semicircle of 2.5 wt% MoS_2/CdS indicated the fast electron transfer due to the excellent conductivity of the introduced $MoS_{2(Qin et al. 2017)}$. The characterization results reflected that the MoS_2/CdS heterojunction improved the separation and transfer efficiency of photon-generated carriers (Xu &Cao 2015, Zhang et al. 2014).

3.2 Effect of different photocatalysts and pH

As shown in Fig. 3a, the no removal of U(VI) was observed in the absence of photocatalysts and light irradiation, which ruled out the possibility of self-photolysis of U(VI) (Wang et al. 2020). Under the dark conditions, the adsorption of U(VI) on photocatalysts slightly increased (from 11.3 to 16.7%) with increasing doping amount of MoS_2, indicating no obvious difference in the adsorption capacity of photocatalysts for U(VI)(Li et al. 2019c). For CdS, the low photocatalytic efficiency of CdS (i.e., ~ 0.6% after 20 min irradiation) was mainly due to the rapid recombination of photogenerated electrons and holes(Dai et al. 2021, Qiu et al. 2021, Zhang et al. 2020b). Within 15 min irradiation, the photocatalytic efficiency of 2.5 wt% MoS_2/CdS (97.51%) was remarkably higher than 10 wt% MoS_2/CdS (65%) due to the reduction of active sites by adding aggregated $MoS_{2(Chen et al. 2019, Zhang et al. 2020a)}$. Fig. 3b shows the

effect of pH on the photoreduction efficiency of U(VI) on 2.5 wt% MoS_2/CdS. Almost no removal of U(VI) at pH 3.0 may be due to the competing of H^+ and U(VI)(He et al. 2017, Zhang et al. 2020b). The highest removal rate of U(VI) (99.64%) was observed at pH 7.0 due to the fast transfer of generated charges of 2.5 wt% MoS_2/CdS under neutral conditions(Dai et al. 2021), which limited the recombination of photogenerated electrons and holes (Li et al. 2019d).

3.3 Effect of U(VI) concentration and dosage

Figure 3c and 3d show the effect of U(VI) concentrations (10, 20 and 30 ppm) and dosage (0.5, 1.0 and 2.0 mg/mL) on U(VI) photoreduction, respectively. Within 5 min irradiation, the highest removal of U(VI) at 20 ppm was consistent with the previous studies(Lei et al. 2021, Zhang et al. 2020b). Similarly, the highest removal efficiency of U(VI) was observed at 1.0 g/L under light irradiation. The further increase of U(VI) concentration and photocatalyst dosage leads to the decrease of U(VI) photoreduction due to the occurrence of shielding effect after exceeding the optimal concentration and dosage(Jiang et al. 2021, Zhang et al. 2021).

3.4 Regeneration and quenching experiments

Figure 4a and 4b show the regeneration and quenching experiments of U(VI) photoreduction on 2.5 wt% MoS_2/CdS, respectively. After 5 times of recycling, 2.5 wt% MoS_2/CdS still exhibited the high photocatalytic removal efficiency (>97%, Fig. 4a). In addition, no change in microstructure and crystal structure was observed after the photocatalytic reduction process (Fig. 1c and 1d). The regeneration results indicated that 2.5 wt% MoS_2/CdS had high photoreduction efficiency, good chemical stability and excellent reusability(Yu et al. 2014). The photoreduction mechanism of U(VI) on 2.5 wt% MoS_2/CdS composites was investigated by quenching experiments. TBA, p- BQ and Me were used as electron acceptors to remove ·OH, $\cdot O_2^-$ and holes, respectively(Jiang et al. 2018, Wang et al. 2019). As shown in Fig. 4b, only 20% of U(VI) was photo-reduced after adding p-BQ into the reaction system, indicating the significant inhibition of photocatalytic activity. The little effect of TBA and Me on U(VI) photoreduction was observed. This experiment confirmed that $\cdot O_2^-$ radicals were responsible for U(VI) photocatalytic reduction (Yuan et al. 2018).

In order to further clarify the reaction mechanism, an electron spin resonance spin trap experiment was performed, which can detect the generation of ·OH and $\cdot O_2^-$ in the light experimental system(Zhang et al. 2021). As displayed in Fig. 4c and Figure S3, no peak and characteristic peaks of DMPO-·OH and DMPO-$\cdot O_2^-$ were observed under the dark and light condition, respectively, indicating that ·OH and $\cdot O_2^-$ were generated at $\lambda > 420$ nm (Gong et al. 2021). Compared to DMPO-·OH, the intensities of DMPO-$\cdot O_2^-$ were significantly weak after adding U(VI), which can be deduced that dissolved oxygen acts as an electron shuttle between 2.5 wt% MoS_2/CdS(Le et al. 2020).

3.5 XPS analysis

XPS analysis was used to determine the photocatalytic reduction of U(VI) on CdS and 2.5 wt% MoS_2/CdS composite. Apart from Cd 3d and S 2p, the appearance of low Mo 3d peak showed the success synthesis of MoS_2/CdS composite (Fig. 5a). In addition, U 4f peak was also found for 2.5 wt% MoS_2/CdS composite after reaction. As shown in Fig. 5b, the two peaks of Mo 3d at 226.0 eV and 232.5 eV corresponded to Mo^{4+} $3d_{5/2}$ and Mo^{4+} $3d_{3/2}$, respectively(Alomar et al. 2019, Jin &Li 2020). After the reaction, Mo^{4+} $3d_{5/2}$ was shifted by +0.2eV, while Mo^{4+} $3d_{3/2}$ had no obvious shift. Similarly, S 2p spectra at 161.8 and 163.0 eV corresponded to S $2p_{3/2}$ and S $2p_{1/2}$, respectively (Fig. 5c). Compared to CdS, the increased binding energy and slight shift (0.1-0.2 eV) of S 2p in 2.5wt% MoS_2/CdS was due to addition of $MoS_{2(Wu et al. 2017)}$. The slight shift of Cd 3d (i.e., Cd $3d_{5/2}$ from 405.2 to 405.4 eV, Cd $3d_{3/2}$ from 411.9 to 412.1 eV, Fig. S4 of SI) was due to the change of Cd 3d orbit caused by the chemical bond(Yuan et al. 2018). For 2.5wt% MoS_2/CdS, the change in binding energy of Cd 3d and S 2p may be likely to accelerate the separation of excited charges of 2.5 wt% MoS_2/CdS under the light irradiation, improving the photocatalytic activity(Yu et al. 2021). U 4f peak at 381.62 and 392.50 eV were assigned to U $4f_{7/2}$ and U $4f_{5/2}$ of U(VI), respectively (Fig. 5d). U $4f_{7/2}$ can be decomposed into two peaks of 380.1 and 381.6 eV, which were attributed to U(VI) and U(IV), respectively(Zhang et al. 2020a). The similarity of U $4f_{5/2}$ peak was also observed, indicating photoreduction of adsorbed U(VI) into U(IV) by photogenerated electrons in a short time(Li et al. 2019d, Wang et al. 2019, Zhang et al. 2020b).

3.6 Mechanism analysis

Based on the above experimental results and band structure theory, the mechanism of catalytic reduction of U(VI) with 2.5 wt% MoS_2/CdS catalyst under all-light is roughly as follows(Chang et al. 2015):

$MoS_2/CdS + hv \rightarrow e^- + h^+$ (1)

$H_2O + h^+ \rightarrow \cdot OH + H^+$ (2)

$CH_3OH + h^+ + \cdot OH \rightarrow CO_2 + H_2O$ (3)

$O_2 + e^- \rightarrow O^-_2$ (4)

$U(VI) + \cdot O^-_2 \rightarrow U(IV) + 2O_2$ (5)

The electrons (e^-) in the valence band (VB) are excited under light irradiation when the light energy is greater than or equal to the band gap of MoS_2/CdS ($hv \geq Eg$)(Gorshkov et al. 2006). Then photogenerated electrons were jumped into the conduction band (CB), an equal number of holes (h^+) are generated in VB (Eqn. 1). The holes of VB and electrons of CB have certain oxidation and reduction ability, respectively(Yin et al. 2016b, Zong et al. 2010). h^+ can react with water to form ·OH radicals (Eqn. 2), and/or h^+ can oxidize organics into CO_2 and H_2O (Eqn. 3). The $\cdot O^-_2$ radicals were generated by reaction of e^- and dissolved O_2 (Eqn. 4). Therefore, the adsorbed U(VI) by the active site of catalyst can be

reduced to U(IV) by $\cdot O^-_2$ (Eqn. 5)(Jiang et al. 2018). The generated O_2 was quickly captured by e^- again (Eqn. 4).

4. Conclusions

In summary, 2.5 wt% MoS2/CdS composite exhibited the high photocatalytic reduction of U(VI) (97.5% within 15 min) and fast reaction equilibrium (complete removal within 30 min) due to the narrow band gap, which can effectively inhibit the recombination of photogenerated electron-hole pairs. The high photocatalytic reduction of U(VI) (~97%) after 5 recycles revealed the chemical stability of MoS_2/CdS composite. XPS analysis indicated that adsorbed U(VI) were reduced to U(IV) by photogenerated electrons. These findings are crucial for the application of CdS-based composite towards the high efficient removal of U(VI) in actual environmental cleanup.

Declarations

Ethical Approval: Not applicable
Consent to Participate: Not applicable.
Consent to Publish: Not applicable.
Competing Interests: The authors declare no competing interests.

Authors Contributions: Jingting Xiao: conceptualization, methodology, investigation, writing and revising original draft. Xinshui Huang: Methodology, editing. Peng Mei: Methodology, Analysis, Editing. Huihui Wang: methodology, Analysis and editing. Yubing Sun: Conceptualization, writing-review, revising, editing, supervision.
Funding The project was financially supported by Fundamental Research Funds of the Central Universities (No. 2021MS036).
Availability of data and materials: All data generated or analyzed during this study are included in this published article.

References

1. Alomar M, Liu Y, Chen W, Fida H (2019) : Controlling the growth of ultrathin MoS_2 nanosheets/CdS nanoparticles by two-step solvothermal synthesis for enhancing photocatalytic activities under visible light.Appl. Surf. Sci.480,1078–1088
2. Andrews MB, Cahill CL (2013) : Uranyl bearing hybrid materials: synthesis, speciation, and solid-state structures.Chem. Rev.113,1121–1136
3. Arunachalam VS, Fleischer EL (2008) : The global energy landscape and materials innovation.Mrs Bull. 33,264–288
4. Gu B, Liang L, Dickey MJ, Yin X, S (1998) : Reductive precipitation of uranium(VI) by zero-valent iron.Environ. Sci. Technol.32,3366–3373

5. Chai B, Xu M, Yan J, Ren Z (2018) : Remarkably enhanced photocatalytic hydrogen evolution over MoS_2 nanosheets loaded on uniform CdS nanospheres.Appl. Surf. Sci.430,523–530
6. Chang K, Li M, Wang T, Ouyang S, Li P, Liu L, Ye J (2015) : Drastic layer-number-dependent activity enhancement in photocatalytic H_2 Evolution over $nMoS_2$/CdS ($n \geq 1$) under visible light.Adv. Energy Mater.5,1–8
7. Chen G, Li D, Li F, Fan Y, Zhao H, Luo Y, Yu R, Meng Q (2012) : Ball-milling combined calcination synthesis of MoS_2/CdS photocatalysts for high photocatalytic H_2 evolution activity under visible light irradiation.Appl. Catal. A-Gen.443,138–144
8. Chen J, Wu X-J, Yin L, Li B, Hong X, Fan Z, Chen B, Xue C, Zhang H (2015) : One-pot synthesis of CdS nanocrystals hybridized with single-layer transition-metal dichalcogenide nanosheets for efficient photocatalytic hydrogen evolution.Angew. Chem. Int. Ed.54,1210–1214
9. Chen K, Chen C, Ren X, Alsaedi A, Hayat T (2019) : Interaction mechanism between different facet TiO_2 and U(VI): experimental and density-functional theory investigation.Chem. Eng. J.359,944–954
10. Chu S, Majumdar A (2012) : Opportunities and challenges for a sustainable energy future.Nature488,294–303
11. Dai Z, Zhen Y, Sun Y, Li L, Ding D (2021) : $ZnFe_2O_4$/g-C_3N_4 S-scheme photocatalyst with enhanced adsorption and photocatalytic activity for uranium(VI) removal.Chem. Eng. J.415,129–135
12. Di T, Zhu B, Zhang J, Cheng B, Yu J (2016) : Enhanced photocatalytic H_2 production on CdS nanorod using cobalt-phosphate as oxidation cocatalyst.Appl. Surf. Sci.389,775–782
13. Dolatyari L, Yaftian MR, Rostamnia S (2016) : Removal of uranium(VI) ions from aqueous solutions using Schiff base functionalized SBA-15 mesoporous silica materials.J. Environ. Manage.169,8–17
14. Gong J, Xie Z, Wang B, Li Z, Zhu Y, Xue J, Le Z (2021) : Fabrication of g-C_3N_4-based conjugated copolymers for efficient photocatalytic reduction of U(VI).J. Environ. Chem. Eng.9,104–111
15. Gorshkov N, Izosimov I, Kolichev S, Smirnov V, Firsin N (2006) : Isotope effect in the photoreduction of UO_2F_2 enriched with O-18 in isopropanol solution.J. Nucl. Sci. Technol.43,407–410
16. Graves C, Ebbesen SD, Mogensen M, Lackner KS (2011) : Sustainable hydrocarbon fuels by recycling CO_2 and H_2O with renewable or nuclear energy.Renew. Sust. Energ. Rev.15,1–23
17. Habibi MH, Rahmati MH (2014) : Fabrication and characterization of ZnO@CdS core–shell nanostructure using acetate precursors: XRD, FESEM, DRS, FTIR studies and effects of cadmium ion concentration on band gap.Spectrochim. Acta A: Mol. Biomol. Spectrosc.133,13–18
18. He J, Chen L, Wang F, Liu Y, Chen P, Au C-T, Yin S-F (2016) : CdS nanowires decorated with ultrathin MoS_2 nanosheets as an rfficient photocatalyst for hydrogen evolution.Chemsuschem9,624–630
19. He Z, Wang D, Tang J, Song S, Chen J, Tao X (2017) : A quasi-hexagonal prism-shaped carbon nitride for photoreduction of carbon dioxide under visible light.Environ. Sci. Pollut. Res.24,8219–8229
20. Jacobson MZ (2009) : Review of solutions to global warming, air pollution, and energy security.Energy Environ. Sci.2,148–173

21. Jacobson MZ, Delucchi MA (2011) : Providing all global energy with wind, water, and solar power, part I: Technologies, energy resources, quantities and areas of infrastructure, and materials.Energ. Policy39,1154–1169
22. Jiang P, Yu K, Yuan H, He R, Sun M, Tao F, Wang L, Zhu W (2021) : Encapsulating Ag nanoparticles into ZIF-8 as an efficient strategy to boost uranium photoreduction without sacrificial agents dagger.J. Mater. Chem. A9,9809–9814
23. Jiang W, Liu Y, Zong R, Li Z, Yao W, Zhu Y (2015) : Photocatalytic hydrogen generation on bifunctional ternary heterostructured $In_2S_3/MoS_2/CdS$ composites with high activity and stability under visible light irradiation.J. Mater. Chem. A3,18406–18412
24. Jiang X-H, Xing Q-J, Luo X-B, Li F, Zou J-P, Liu S-S, Li X, Wang X-K (2018) : Simultaneous photoreduction of uranium(VI) and photooxidation of arsenic (III) in aqueous solution over g-C_3N_4/TiO_2 heterostructured catalysts under simulated sunlight irradiation.Appl. Catal. B-Environ.228,29–38
25. Jin X, Li G (2020) : Synthesis of MoS_2/CdS nanospheres enhanced photocatalytic hydrogen evolution under visible light.J. Mater. Sci. Mater. Electron.31,9377–9384
26. Khawula TNY, Raju K, Franklyn PJ, Sigalas I, Ozoemena KI (2016) : Symmetric pseudocapacitors based on molybdenum disulfide (MoS_2)-modified carbon nanospheres: correlating physicochemistry and synergistic interaction on energy storage.J. Mater. Chem. A4,6411–6425
27. Le Z, Xiong C, Gong J, Wu X, Pan T, Chen Z, Xie Z (2020) : Self-cleaning isotype g-C_3N_4 heterojunction for efficient photocatalytic reduction of hexavalent uranium under visible light.Environ. Pollut.260,456–459
28. Lei J, Liu H, Yuan C, Chen Q, Liu J-A, Wen F, Jiang X, Deng W, Cui X, Duan T, Zhu W, He R (2021) : Enhanced photoreduction of U(VI) on WO_3 nanosheets by oxygen defect engineering.Chem. Eng. J.416,129–125
29. Li LL, Yin XL, Pang DH, Du XX, Xue H, Zhou HW, Yao QX, Wang HW, Qian JC, Yang J, Li DC, Dou JM (2019a) : One-pot synthesis of MoS_2/CdS nanosphere heterostructures for efficient H_2 evolution under visible light irradiation.Int. J. Hydrog. Energy44,31930–31939
30. Li LL, Yin XL, Sun YQ (2019b) : Facile synthesized low-cost MoS_2/CdS nanodots-on-nanorods heterostructures for highly efficient pollution degradation under visible-light irradiation.Sep. Purif. Technol.212,135–141
31. Li P, Wang J, Peng T, Wang Y, Liang J, Pan D, Fan Q (2019c) : Heterostructure of anatase-rutile aggregates boosting the photoreduction of U(VI).Appl. Surf. Sci.483,670–676
32. Li P, Wang J, Wang Y, Liang J, He B, Pan D, Fan Q, Wang X (2019d) : Photoconversion of U(VI) by TiO_2: An efficient strategy for seawater uranium extraction.Chem. Eng. J.365,231–241
33. Li Y, Wang L, Li B, Zhang M, Wen R, Guo X, Li X, Zhang J, Li S, Ma L (2016) : Pore-free matrix with cooperative chelating of hyperbranched ligands for high-performance separation of uranium.ACS Appl. Mater. Inter.,28853–28861

34. Lin H, Li Y, Li H, Wang X (2017) : Multi-node CdS hetero-nanowires grown with defect-rich oxygen-doped MoS_2 ultrathin nanosheets for efficient visible-light photocatalytic H_2 evolution.Nano Res.10,1377–1392
35. Liu Y, Yu Y-X, Zhang W-D (2013) : MoS_2/CdS heterojunction with high photoelectrochemical activity for H_2 evolution under visible Light: the role of MoS_2.J. Phys. Chem. C117,12949–12957
36. Misra SK, Mahatele AK, Tripathi SC, Dakshinamoorthy A (2009) : Studies on the simultaneous removal of dissolved DBP and TBP as well as uranyl ions from aqueous solutions by using micellar-enhanced ultrafiltration technique.Hydrometallurgy96,47–51
37. Qin N, Xiong J, Liang R, Liu Y, Zhang S, Li Y, Li Z, Wu L (2017) : Highly efficient photocatalytic H_2 evolution over MoS_2/CdS-TiO_2 nanofibers prepared by an electrospinning mediated photodeposition method.Appl. Catal. B-Environ.202,374–380
38. Qiu M, Liu Z, Wang S, Hu B (2021) : The photocatalytic reduction of U(VI) into U(IV) by ZIF-8/g-C_3N_4 composites at visible light.Environ. Res.196,23–30
39. Sing K, Everett DH, Haul R, Moscou L, Siemieniewska T (1985) : Reporting physisorption data for gas/solid system, 57.*Handbook of Heterogeneous Catalysis*
40. Wang H, Guo H, Zhang N, Chen Z, Hu B, Wang X (2019) : Enhanced photoreduction of U(VI) on C_3N_4 by Cr(VI) and bisphenol A: ESR, XPS, and EXAFS investigation.Environ. Sci. Technol.53,6454–6461
41. Wang Z, Xu S-M, Tan L, Liu G, Shen T, Yu C, Wang H, Tao Y, Cao X, Zhao Y, Song Y-F (2020) : 600 nm-driven photoreduction of CO_2 through the topological transformation of layered double hydroxides nanosheets.Appl. Catal. B-Environ.270,118–126
42. Wu A, Tian C, Jiao Y, Yan Q, Yang G, Fu H (2017) : Sequential two-step hydrothermal growth of MoS_2/CdS core-shell heterojunctions for efficient visible light-driven photocatalytic H_2 evolution.Appl. Catal. B-Environ.203,955–963
43. Xie J, Zhang H, Li S, Wang R, Sun X, Zhou M, Zhou J, Lou XW, Xie Y (2013a) : Defect-Rich MoS_2 ultrathin nanosheets with additional active edge sites for enhanced electrocatalytic hydrogen evolution.Adv. Mater.25,5807–5813
44. Xie J, Zhang J, Li S, Grote F, Zhang X, Zhang H, Wang R, Lei Y, Pan B, Xie Y (2013b) : Controllable disorder engineering in oxygen-incorporated MoS_2 ultrathin nanosheets for efficient hydrogen evolution.J. Am. Chem. Soc.135,17881–17888
45. Xu J, Cao X (2015) : Characterization and mechanism of MoS_2/CdS composite photocatalyst used for hydrogen production from water splitting under visible light.Chem. Eng. J.260,642–648
46. Yan HJ, Yang JH, Ma GJ, Wu GP, Zong X, Lei ZB, Shi JY, Li C (2009) : Visible-light-driven hydrogen production with extremely high quantum efficiency on Pt-PdS/CdS photocatalyst.J. Catal.266,165–168
47. Yin X-L, He G-Y, Sun B, Jiang W-J, Xue D-J, Xia A-D, Wan L-J, Hu J-S (2016a) : Rational design and electron transfer kinetics of MoS_2/CdS nanodots-on-nanorods for efficient visible-light-driven hydrogen generation.Nano Energy28,319–329

48. Yin X-L, Li L-L, Jiang W-J, Zhang Y, Zhang X, Wan L-J, Hu J-S (2016b) : MoS_2/CdS nanosheets-on-nanorod heterostructure for highly efficient photocatalytic H_2 generation under visible light irradiation.ACS Appl. Mater. Inter.8,15258–15266
49. Yu J, Jin J, Cheng B, Jaroniec M (2014) : A noble metal-free reduced graphene oxide–CdS nanorod composite for the enhanced visible-light photocatalytic reduction of CO_2 to solar fuel.J. Mater. Chem. A2,3407–3416
50. Yu K, Jiang P, Yuan H, He R, Zhu W, Wang L (2021) : Cu-based nanocrystals on ZnO for uranium photoreduction: plasmon-assisted activity and entropy-driven stability.Appl. Catal. B-Environ.288,119–126
51. Yuan Y-J, Li Z, Wu S, Chen D, Yang L-X, Cao D, Tu W-G, Yu Z-T, Zou Z-G (2018) : Role of two-dimensional nanointerfaces in enhancing the photocatalytic performance of 2D-2D MoS_2/CdS photocatalysts for H_2 production.Chem. Eng. J.350,335–343
52. Zhang J, Zhu Z, Feng X (2014) : Construction of two-dimensional MoS_2/CdS p-n nanohybrids for highly efficient photocatalytic hydrogen evolution.Chem. Eur. J.20,10632–10635
53. Zhang X-H, Li N, Wu J, Zheng Y-Z, Tao X (2018) : Defect-rich O-incorporated 1T-MoS_2 nanosheets for remarkably enhanced visible-light photocatalytic H_2 evolution over CdS: The impact of enriched defects.Appl. Catal. B-Environ.229,227–236
54. Zhang Y, Zhu M, Zhang S, Cai Y, Lv Z, Fang M, Tan X, Wang X (2020a) : Highly efficient removal of U(VI) by the photoreduction of SnO_2/$CdCO_3$/CdS nanocomposite under visible light irradiation.Appl. Catal. B-Environ.279,119–126
55. Zhang Z, Dong Z, Wang X, Dai Y, Cao X, Wang Y, Hua R, Feng H, Chen J, Liu Y, Hu B, Wang X (2019) : Synthesis of ultralight phosphorylated carbon aerogel for efficient removal of U(VI): Batch and fixed-bed column studies.Chem. Eng. J.370,1376–1387
56. Zhang Z, Liu C, Dong Z, Dai Y, Xiong G, Liu Y, Wang Y, Wang Y, Liu Y (2020b) : Synthesis of flower-like MoS_2/g-C_3N_4 nanosheet heterojunctions with enhanced photocatalytic reduction activity of uranium(VI).Appl. Surf. Sci.520,45–52
57. Zhang Z, Zhou R, Dong Z, Wu Y, Xu L, Xie Y, Li Z, Xiong Y, Wang Y, Liu Y (2021) : Visible-light induced photocatalytic removal of U(VI) from aqueous solution by MoS_2/g-C_3N_4 nanocomposites.J. Radioanal. Nucl. Chem.328,9–17
58. Zong X, Yan H, Wu G, Ma G, Wen F, Wang L, Li C (2008) : Enhancement of photocatalytic H_2 evolution on CdS by loading MoS_2 as cocatalyst under visible light irradiation.J. Am. Chem. Soc.130,7176–7181
59. Zong X, Wu G, Yan H, Ma G, Shi J, Wen F, Wang L, Li C (2010) : Photocatalytic H_2 Evolution on MoS_2/CdS Catalysts under Visible Light Irradiation.J. Phys. Chem. C114,1963–1968

Figures

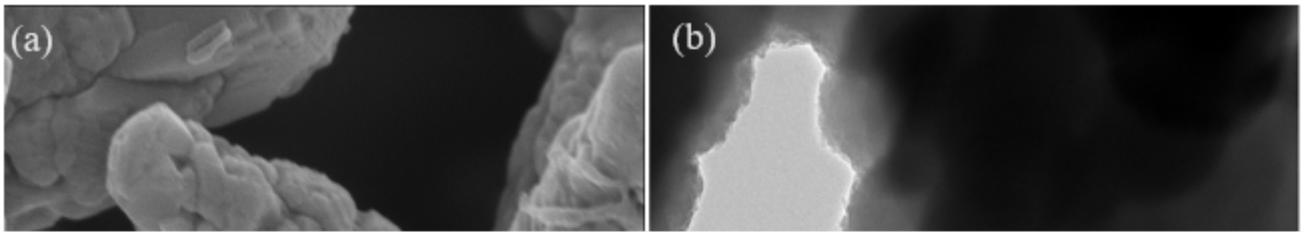

Figure 1

Characterization of MoS2/CdS. (a): SEM of CdS; (b): TEM of 2.5 wt% MoS2/CdS; (c): XRD patterns of CdS, 2.5, 5 and 10 wt % MoS2/CdS; (d): FT-IR spectra of 2.5 wt% MoS2/CdS before and after reaction.

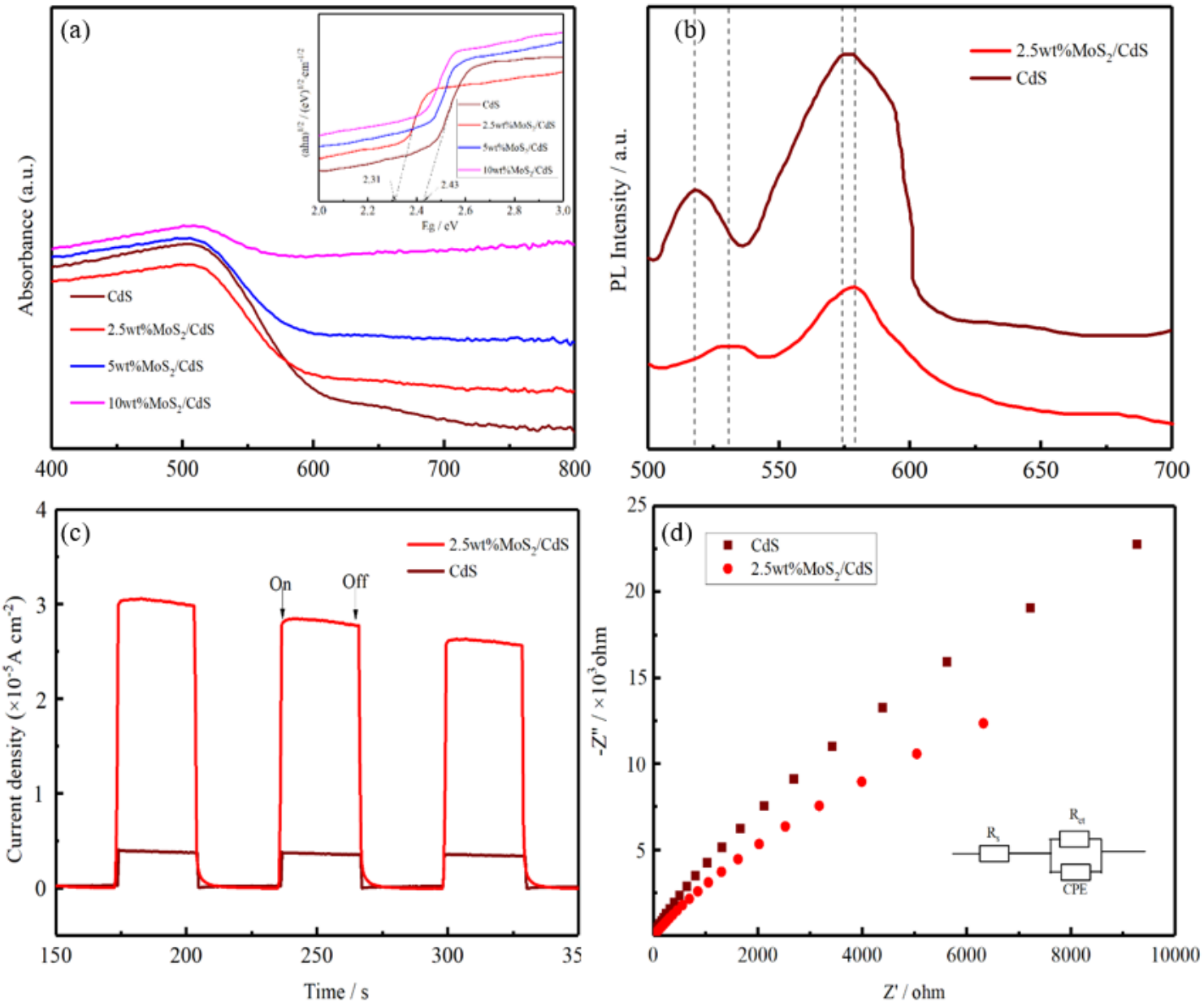

Figure 2

Spectroscopic and electrochemical properties of MoS2/CdS. (a): UV-vis absorbance spectra of CdS , 2.5, 5 and 10 wt% MoS2/CdS, and inset of band gap by Kubelka–Munk model; (b), (c) and (d): PL spectra, Transient photocurrent responses and EIS Nyquist plots, respectively.

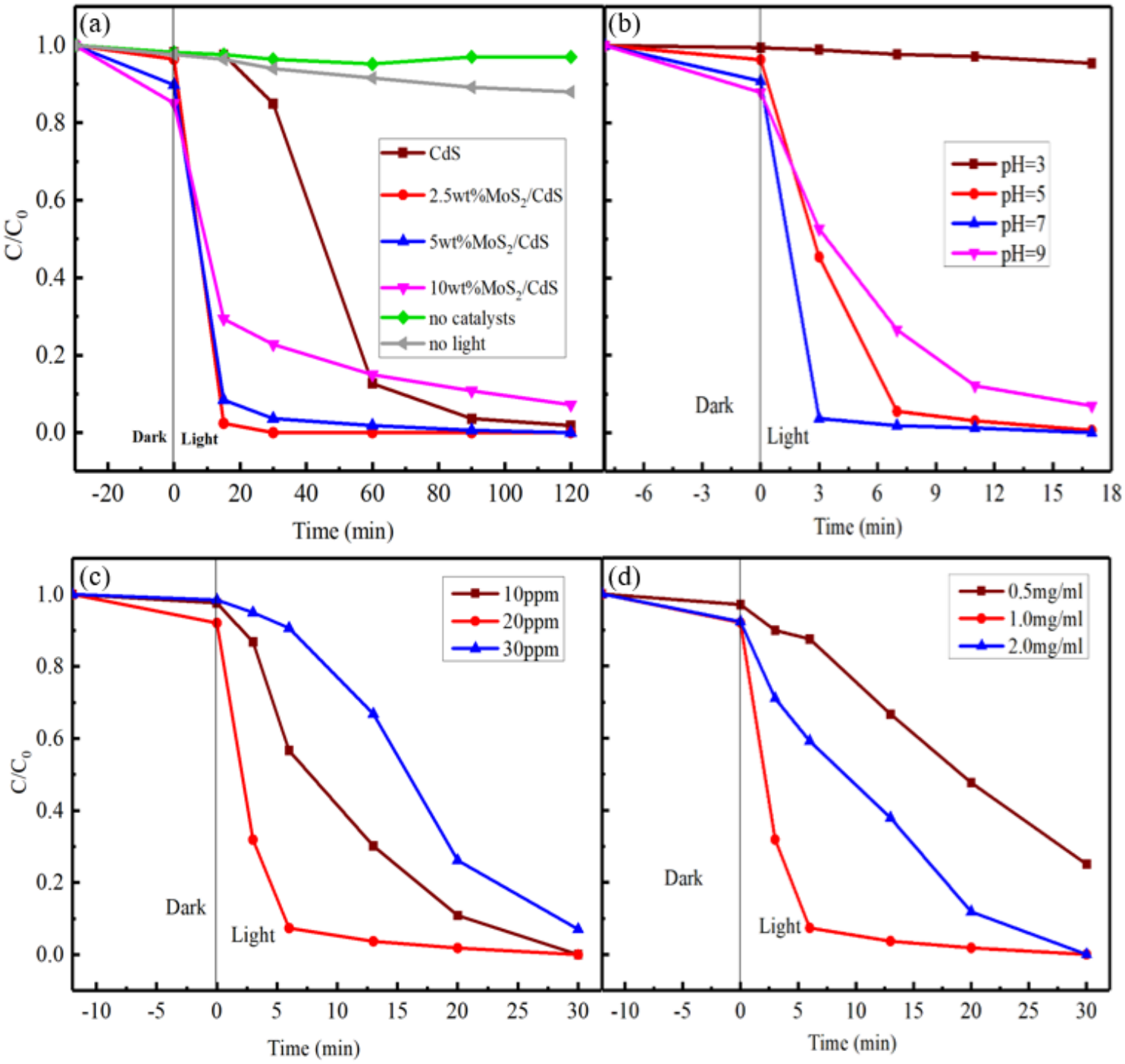

Figure 3

Photocatalytic reduction of U (VI) on MoS2/CdS photocatalysts. (a) and (b): effect of different photocatalyst and pH, respectively; (c) and (d): effect of U(VI) concentration and dosage, respectively, CU(VI) = 20 mg/L, pH 6.

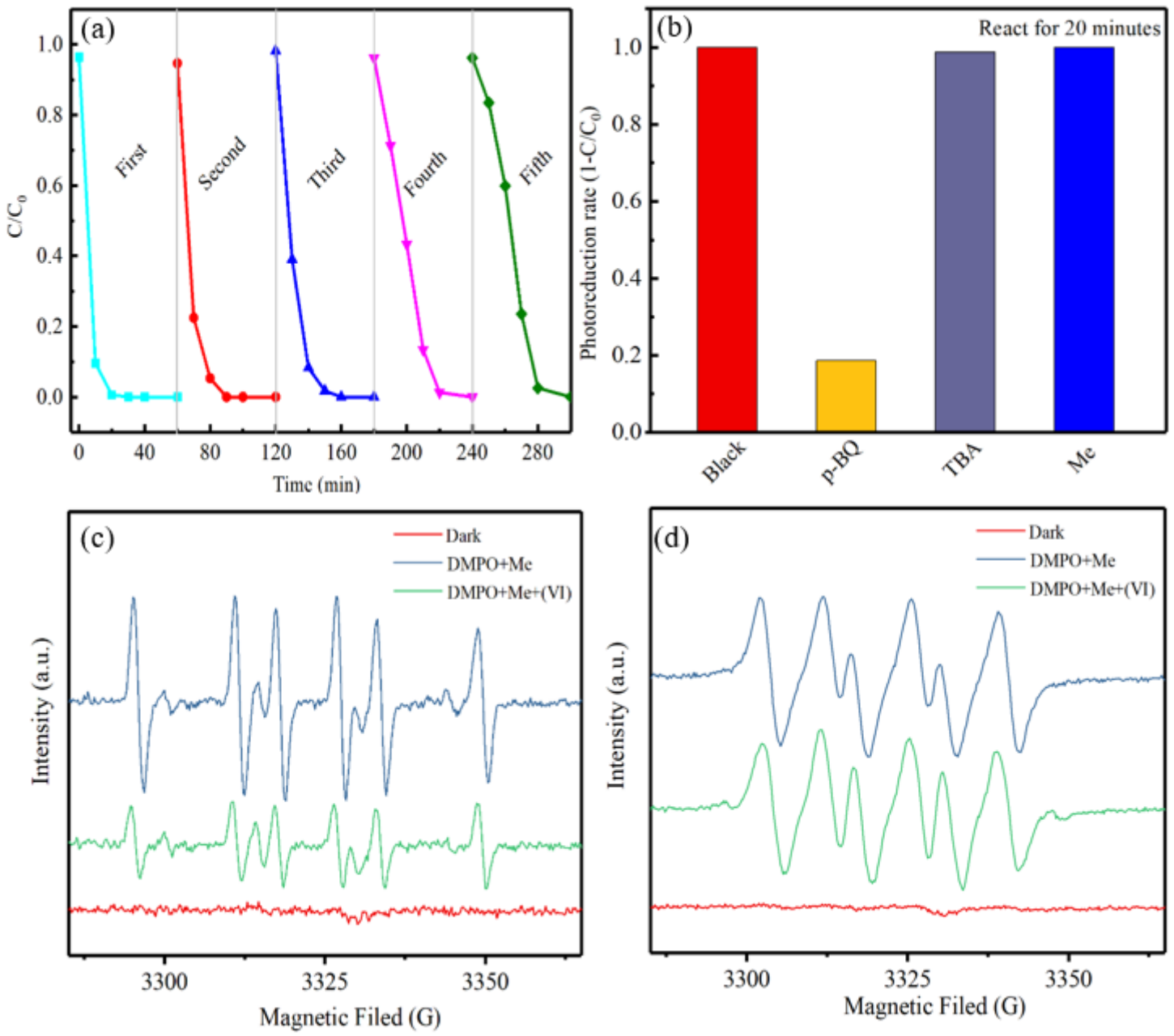

Figure 4

(a): regeneration of U(VI) photocatalytic reduction on 2.5 wt% MoS2/CdS composites; (b): quenching experiments of U(VI) on 2.5 wt% MoS2/CdS. (c): ESR spectra of DMPO-·OH and (d): DMPO-·O2- with the dark/light irradiation.

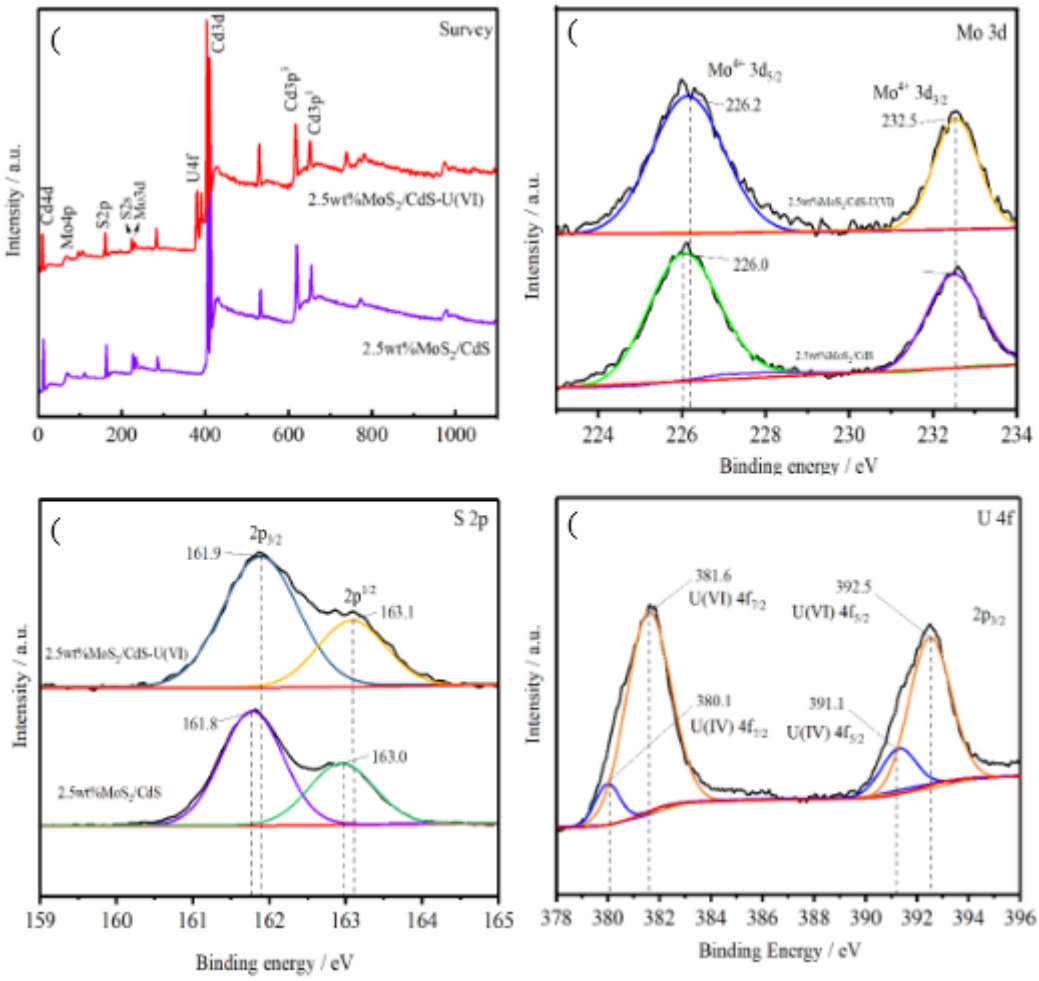

Figure 5

XPS analysis of CdS, 2.5 wt% MoS2/CdS before and after reaction, (a) total scan, (b), (c) and (d): Mo 3d, S 2p and U 4f XPS spectra, respectively.

Supplementary Files

This is a list of supplementary files associated with this preprint. Click to download.

- SI20210805.docx